

# Loss-resilient Coding of Texture and Depth for Free-viewpoint Video Conferencing

Bruno Macchiavello, Camilo Dorea, Edson M. Hung, Gene Cheung *Senior Member, IEEE* and Wai-tian Tan *Senior Member, IEEE*

**Abstract**—Free-viewpoint video conferencing allows a participant to observe the remote 3D scene from any freely chosen viewpoint. An intermediate virtual viewpoint image is commonly synthesized using two pairs of transmitted texture and depth maps from two neighboring captured viewpoints via depth-image-based rendering (DIBR). To maintain high quality of synthesized images, it is imperative to contain the adverse effects of network packet losses that may arise during texture and depth video transmission. Towards this end, we develop an integrated approach that exploits the representation redundancy inherent in the multiple streamed videos—a voxel in the 3D scene visible to two captured views is sampled and coded twice in the two views. In particular, at the receiver we first develop an error concealment strategy that adaptively blends corresponding pixels in the two captured views during DIBR, so that pixels from the more reliable transmitted view are weighted more heavily. We then couple it with a sender-side optimization of reference picture selection (RPS) during real-time video coding, so that blocks containing samples of voxels that are visible in both views are more error-resiliently coded in one view only, given adaptive blending will erase errors in the other view. Further, synthesized view distortion sensitivities to texture versus depth errors are analyzed, so that relative importance of texture and depth code blocks can be computed for system-wide RPS optimization. Experimental results show that the proposed scheme can outperform the use of a traditional feedback channel by up to 0.82 dB on average at 8% packet loss rate, and by as much as 3 dB for particular frames.

**Index Terms**—Free viewpoint video conferencing, reference picture selection, error concealment, depth-image-based rendering.

## I. INTRODUCTION

THE demand for ever improving quality of video communication has already made high definition video conferencing a basic feature not only on computers, but smart-phones as well. A free-viewpoint video conferencing system [1] that continuously alters the displayed images according to a user's real-time selected viewpoints—e.g., through *motion parallax* [2], where detected head movements trigger corresponding rendering of images as viewed from the observer's viewpoint—can enhance an observer's depth perception in the 3D scene, and bring video communication to a new level

of immersion and realism. The techniques for capturing [3], representing [4], [5], and synthesizing [6], [7] free-viewpoint video have been well studied. Instead, in this paper we address the problem of robust low-latency streaming of free-viewpoint video over packet-loss prone networks.

We adopt the widely employed depth-image-based rendering (DIBR) approach [7] to provide free viewpoint. As the name suggests, in addition to typical RGB images (texture), DIBR requires also depth images (per-pixel physical distances between captured objects in the 3D scene and capturing camera) to synthesize a freely chosen viewpoint image. Depth maps can be obtained by estimation algorithms like stereo-matching, or depth sensors like time-of-flight cameras [8]. While recent proposals such as [9], [10] suggest transmission of one pair of texture and depth maps from a single camera-captured viewpoint for synthesis of a defined neighborhood of viewpoints, this usually leads to larger disoccluded regions<sup>1</sup> in the synthesized view that require image inpainting [11], [12] to complete the image, resulting in high complexity. We hence assume the more customary approach of transmitting texture and depth maps of two neighboring captured views [2], [13] to ensure quality reconstruction of freely chosen intermediate virtual views.

The transport of texture and depth videos for multiple views presents both challenges and opportunities. On one hand, the complex dependency of rendered view quality on both depth and texture maps of captured views needs to be adequately modeled to realize effective error-resilience measures. On the other hand, the inherent representation redundancy in multiple texture-plus-depth videos—a voxel<sup>2</sup> in the 3D scene visible to two captured views is sampled and coded twice in the two views—suggests that errors in one view can be ameliorated by correct delivery of another view. Towards this end, we develop an integrated approach in this paper where receiver and sender are jointly designed to exploit and manipulate the inherent representation redundancy present in depth and texture videos from multiple views. To the best of our knowledge, this is the first work in the literature that exploits representation redundancy in multiple texture-plus-depth videos for loss-resilient streaming.

To exploit representation redundancy at the receiver, we first develop an error model that tracks the reliability of

Bruno Machiavello, Camilo Dorea, Edson M. Hung are with the University of Brasilia - Asa Norte, CEP: 70910-900, Brasilia - DF, Brazil  
Email Address: {bruno, camilo, mintsu}@image.unb.br.

Gene Cheung is with the National Institute of Informatics, 2-1-2, Hitotsubashi, Chiyoda-ku, Tokyo, 101-8430, Japan  
Email Address: cheung@nii.ac.jp.

Wai-tian Tan is with the Hewlett-Packard Laboratories, 1501 Page Mill Road, Palo Alto, CA 94304, USA  
Email Address: wai-tian.tan@hp.com.

<sup>1</sup>Disoccluded region is a spatial region in the synthesized view with no corresponding pixels in the reference views during DIBR. This issue is discussed in details in Section IV.

<sup>2</sup>A voxel is a volume element representing a value on a regular grid in 3D space [14].

each code block in each transmitted view given observed packet loss events. During DIBR-based rendering of a virtual view, where a synthesized pixel is typically computed as a convex combination of the two corresponding pixels in the two captured views, we perform *adaptive blending*, so that the corresponding pixel from the more reliable transmitted view is assigned a heavier weight. Adaptive blending uniquely targets quality improvement of the DIBR synthesized view, and is thus complementary to conventional error concealment methods that improve reconstruction quality of individual captured views [15], [16].

To exploit representation redundancy at the sender, we design an optimization of reference picture selection (RPS) during real-time video coding, so that blocks containing samples of voxels that are visible in both views are more error-resiliently coded (e.g., through intra-coding or using a reference block in a previous frame that has been acknowledged) in one view only. This is possible because aforementioned adaptive blending is performed at decoder, suppressing errors in one view if corresponding blocks in the other view are correctly delivered. The expected reconstructed error of a block predicted from a given past frame is computed via a set of recursive equations we derive with computation efficiency in mind.

Finally, because depth maps are auxiliary information that only aid in the construction of the synthesized views but are not themselves directly observed, the synthesized view distortion sensitivities to errors in depth maps are clearly different to errors in texture maps. To guide preferential protection, we analyze synthesized view distortion sensitivities to texture versus depth errors, so that relative importance of texture and depth code blocks can be computed for system-wide RPS optimization.

We summarize our texture-plus-depth video streaming optimization for free-viewpoint conferencing as follows:

- 1) At receiver, adaptive blending is performed so that the corresponding pixels from the more reliable transmitted view are weighted more heavily during DIBR-based view synthesis.
- 2) At sender, we perform per-block RPS, so that the expected error, stemming from error propagation of a lost reference block, computed using a set of computation-efficient recursive equations, is minimized for blocks containing important pixels vital to adaptive blending at receiver.
- 3) Synthesized view distortion sensitivities to errors in texture versus depth maps are analyzed, so that preferential RPS for coding of texture and depth blocks can be optimized.

Experimental results show that the proposed scheme can outperform the use of a traditional feedback channel by up to 0.82 dB on average at 8% packet loss rate, and by as much as 3 dB for particular frames.

The rest of the paper is organized as follows. We first discuss related work in Section II. We then overview our streaming system in Section III. We discuss our receiver error concealment strategy using adaptive blending in Section IV. We discuss our sender RPS optimization in Section V. In

Section VI, an analysis of the added computational load of our proposed algorithms is presented. Finally, experimental results and conclusions are presented in Section VII and VIII, respectively.

## II. RELATED WORK

We divide the discussion of related work into four sections. We first discuss related work in multiview and free-viewpoint video coding. We next discuss depth map denoising work in the compression and view synthesis literature. We then discuss related work in error-resilient video streaming and error concealment for conventional 2D video. Finally, we juxtapose the contributions of this paper to our own earlier work on the same topic.

### A. Multiview and Free Viewpoint Video Coding

Multiview video coding (MVC) is concerned with the compression of texture videos captured from multiple nearby viewpoints. Early works in MVC [4], [17] focused on exploiting signal redundancy across view using *disparity compensation* for coding gain—matching of code blocks between neighboring view pictures for efficient signal prediction. Best-matched block in the reference frame is identified by a *disparity vector*, similar to motion vector in motion compensation used in conventional 2D video coding standards like H.263 [18] and H.264 [19]. However, given temporal redundancy has already been exploited via motion compensation, and neighboring temporal frames tend to be more similar than neighboring inter-view frames due to typical high-frame-rate videos captured by cameras, it was shown that additional coding gain afforded by disparity compensation is noticeable but not dramatic (about 1dB difference in PSNR [17]). Given our goal is loss-resilient video streaming, to avoid potential inter-view error propagation in disparity compensated multiview video, we perform motion estimation / compensation independently in each view. (We note further that having independent encoders for different views fits the *multiterminal video coding* paradigm [20], which, besides benefits of lower overall encoding complexity, holds promises of better compression performance in the future via distributed source coding theory.)

While MVC offers view-switches at receiver only among the discrete set of captured and coded views, transmitting both texture and depth videos of nearby views—known as “texture-plus-depth” format [5]—enables the observer to choose any intermediate virtual view for DIBR-based image rendering and display. Given compression of texture maps has been well studied in the past decades (e.g., coding standards such as H.263 [18] and H.264 [19]), much recent works thus focused specifically on depth map compression. These works can be divided into three classes. The first class [21]–[23] designed specific coding tools (e.g., graph-based transform (GBT) [21], [23]) that tailored to the unique signal characteristics of depth maps, such as sharp edges and smooth interior surfaces. In our streaming system, for simplicity we assume H.264 is employed for standard-compliant compression of texture and depth videos in each captured view. However, we note that new coding tools such as GBT can be incorporated into our

streaming optimization easily, if standard-compliant solution is not required.

The second class [24]–[28] observed that a depth map is a source of auxiliary information that assists in the synthesized view construction at decoder, but is itself never directly observed. Thus, one can design coding optimizations that minimize the indirect synthesized view distortion rather than the direct depth map distortion. Our analysis of synthesized view distortion sensitivities to errors in texture and depth maps is an extension of [27] from coding optimization to loss-resilient streaming optimization.

The third class [29], [30] exploited correlations between texture and depth maps of the same view (such as common edge patterns) for compression gain. In our previous study [31], we have concluded that an important depth block (e.g., one that contains an edge between a foreground object and background) can be more critical to synthesized view quality than a texture block. Predicting depth blocks from corresponding texture blocks (as done in [29] as an extension of HEVC video coding standard to texture-plus-depth format) would entail unnatural dependency of a more important depth block on a less important texture block. Given depth video typically requires roughly 10% of the total bitrate and the goal is loss resiliency of free viewpoint video streaming, we choose to forego inter-component prediction and code texture and depth videos of the same view independently using H.264.

### B. Depth Map Denoising

It is observed in the depth map compression and view synthesis literature that multiple depth maps across different views may not be consistent due to acquisition errors and/or compression artifacts. Thus, to eliminate inter-view inconsistency, one can perform pre-processing of depth maps at encoder before compression for coding gain [32], or post-processing at decoder after decoding for improvement in view synthesis quality [33], [34]. In general, the cause of the inconsistency cannot be determined during processing, however, and so when left and right depth maps are in conflict, one cannot determine which one (or both) should be corrected for inter-view consistency. In contrast, in our free-viewpoint video streaming application, the decoder can track the packet loss events to determine the reliability of the left map versus the right map (see Section IV for details). Thus, during DIBR view synthesis an adaptive blending procedure can be applied to assign heavier weight to the corresponding pixel that is more reliable.

### C. Error-resilient Video Streaming

The problem of error control and concealment has been actively studied for many years, and an overview of general approaches can be found in [35]. One particular effective mechanism to control error propagation for systems with live encoder is reference picture selection (RPS). In *reactive* RPS, a live encoder reacts to receiver feedbacks by avoiding the use of notified loss-affected past frames as reference for coding of future frames. In *proactive* RPS, long prediction chains are avoided during video encoding without incorporating real-time

client feedback information. Both reactive and proactive RPS can be implemented to be compatible with video syntax of H.263 version 2, MPEG-4 and H.264. Reactive RPS incurs higher bit overhead only when needed, but suffers error propagation of up to one round-trip time (RTT) at decoder. Proactive RPS incurs an overhead regardless of whether there are actually losses, and should only be applied preferentially to more important parts of the video. A study of adaptively choosing different RPS approaches in streaming of single-view H.264 video is given in [36]. In contrast, we employ at sender proactive RPS with feedbacks [37] (call *proactive-feedback* in the sequel) for selected code blocks in the depth and texture sequences during real-time video encoding, so that the likelihood of long error propagation—typical in differentially coded video—is minimized for blocks containing pixels vital to adaptive rendering at receiver. Our proactive-feedback approach integrates feedback by computing estimated distortion for all frames with and without known loss information.

There are many other techniques developed for improving resilience of single-view video, including error concealment, retransmissions and use of error correcting codes. In addition to commonly employed Reed-Solomon codes, there are also recent low-delay “streaming codes” that allows fast recovery of earlier transmitted packets without requiring all losses to be corrected [38]. Modern video compression formats also have syntax support for error resilience. For example, flexible macroblock ordering [39] is an effective error resilient tool in H.264 that can avoid loss of large contiguous regions to make error concealment more effective. Another example is data partitioning [40], which allows decomposition of compressed single-view video into layers of different importance for preferential protection, and has been implemented in Google’s desktop Chrome browser as part of the WebRTC stack. Furthermore, it is possible to explicitly transmit addition data in various forms to aid error concealment [41].

Many of these techniques are applicable to free-viewpoint conferencing and are complementary to multi-view error concealment methods as well as to adaptive error-resilient source coding methods. To limit the scope of this paper, however, we do not explicitly consider special methods to conceal individual transmitted views nor do we employ retransmissions or error correction codes.

Joint optimization of compression, concealment, and channel loss has also been considered. For example, the work in [42], considers a formulation that allocates transmission power to jointly optimize the average and variance of distortion for single view video. Finally, though there have been streaming optimizations proposed in the literature for stereoscopic video [43] and multiview video [44], to the best of our knowledge we are the first to propose loss-resilient coding specifically for interactive free-viewpoint video where texture and depth maps of two neighboring camera viewpoints are transmitted [45]. In particular, leveraging on the observation that the representation of multiple texture-plus-depth is inherent redundant, we design adaptive blending for view synthesis at decoder and optimized RPS coding scheme at encoder for optimal end-to-end streaming performance.

#### D. Contribution over Our Previous Work

In [46], a similar scheme to minimize expected synthesized view distortion based on selection of reference frame at the block level was proposed for depth maps only. In another previous work [31], we extended the idea in [46] to encoding of both texture *and* depth maps. We also expanded the coding modes available to each MB to include intra block coding. Furthermore, we proposed an optimization algorithm for encoding of both texture and depth maps that nonetheless remains computationally efficient. We note that the recursive model to estimate distortion of a synthesized block using both texture and depth information is inspired by derivations proposed in [47]. We have also studied optimized strategy for motion compensated video in an RPS framework for single-view video at the frame level [37].

In this work, we make significant contributions over our earlier works *by exploiting the inherent representation redundancy in multiple texture-plus-depth videos—a voxel in the 3D scene visible to two captured views is sampled and coded twice in the two views*. Specifically, given the intermediate virtual view is obtained by interpolating texture of two neighboring captured views, an error concealment strategy can be performed during view synthesis where the corresponding pixel with higher reliability is weighted more heavily during pixel blending. Correspondingly, the encoder can perform an optimization algorithm so that pixels that are visible from both captured views can be unequally protected: only pixels from one view are heavily protected to ensure good synthesized pixels at decoder. Note that in this newly updated encoding algorithm, the expected synthesized view distortion depends on the expected error from both coded views. However, we design a novel problem formulation, so that there is no interdependency between frames of the same time instant in both views, easing the system-wide RPS optimization.

### III. REAL-TIME FREE VIEWPOINT VIDEO STREAMING SYSTEM

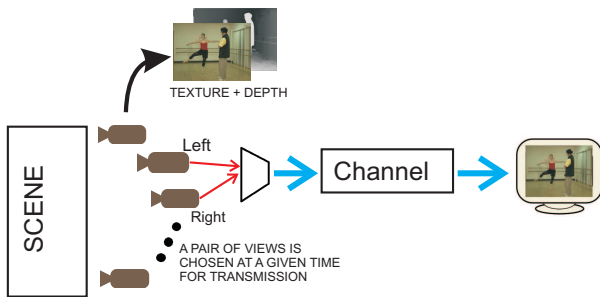


Fig. 1. A bandwidth-efficient free-viewpoint video streaming system dynamically selects two views for transmission.

We overview our proposed real-time free viewpoint video streaming system in this section. At sender, we assume a large array of closely spaced cameras are capturing videos of a 3D scene simultaneously. See Fig. 1 for an illustration. Specific constraints are commonly imposed upon scene acquisition in order to support this application as well as other 3D video services. Cameras are deployed in a 1D parallel arrangement

with narrow acquisition angles and a baseline between cameras of the order of 5 cm [48]. Rectification, performed prior to encoding, is often necessary to eliminate misalignments and provide views in linear and parallel arrangement. These conditions guarantee that disparities between views are limited to 1D shifts along the x-axis. Naturally, accuracy in camera calibration parameters is also required. Furthermore, color consistency among cameras should be assured upon capturing and/or enforced through image processing methods [49] prior to encoding.

Besides texture maps (e.g., color images like RGB), we assume depth maps (per-pixel physical distances between capturing camera and the captured objects in the 3D scene) of the same resolution and from the same camera viewpoints as the texture maps can also be obtained, either via stereo-matching algorithms using neighboring texture maps, or captured directly using depth-sensing cameras [8]. The assumption that both texture and depth maps are available from the same camera viewpoints is a common one for 3D visual data represented in the now popular texture-plus-depth format [5]. Armed with both texture and depth maps, intermediate virtual views can be synthesized via a depth-image-based rendering (DIBR) technique like 3D warping [50], enabling user to select and render image at any desired viewpoint for observation. The ability to choose any viewpoint for image rendering is called *free viewpoint* [49].

The number of cameras capturing video at the same time can be quite large—up to 100 cameras were used in [3]. Hence real-time encoding and transmitting all of them from sender to receiver would translate to too large of a network cost. Instead, we assume here that the current view  $v$  that the receiver is observing is constantly fed back to the sender. The sender can then estimate the range of virtual views the receiver will choose and observe during the next round-trip time (RTT), and then select only *two* neighboring camera views that can enable rendering of those virtual views for real-time coding and transmission of the corresponding texture and depth maps. This idea of selecting only a subset of camera captured views for efficient network transmission is also exploited in [13]. In this paper, we focus on the optimal transmission and error concealment of the texture and depth maps from those two selected views.

### IV. ERROR CONCEALMENT STRATEGY FOR DIBR-BASED SYNTHESIS

We first review a common DIBR view synthesis procedure that assumes no information loss in either depth or texture maps. We then derive formulas for estimates of texture and disparity error for every macroblock (MB) due to packet losses in motion-compensated video. Finally, we discuss how an error concealment strategy for the synthesized view—*adaptive blending*—can be performed given the estimated texture and disparity errors.

#### A. Standard Loss-free View Synthesis

In a multiview DIBR system, an intermediate virtual view is interpolated using texture and depth maps of two neighboring

captured views via a DIBR technique like 3D warping [50]. We focus on the fundamental view blending step upon which our proposal is based. Note that prior to blending, mechanisms aimed at robustness, such as consistency checks, may condition the correspondences among views. The reader is referred to [7] for a complete description of view synthesis procedures.

As a convention, we label left and right views as 0 and 1, respectively. Given the texture map of the left view  $X_t^0$  and right view  $X_t^1$  at time  $t$ , the pixel value  $S_t^v(i, j)$  at coordinate  $(i, j)$  of a synthesized view  $v$  depends on whether we can find a corresponding pixel  $(i, j^0)$  from the left view and a corresponding pixel  $(i, j^1)$  from the right view. Specifically, the synthesized image of view  $v$ ,  $0 \leq v \leq 1$ , has pixel value  $S_t^v(i, j)$  at coordinate  $(i, j)$  given by:

$$S_t^v(i, j) = \begin{cases} (1-v)X_t^0(i, j^0) + vX_t^1(i, j^1) & \text{if L \& R pixels exist} \\ X_t^0(i, j^0) & \text{if only L pixel exists} \\ X_t^1(i, j^1) & \text{if only R pixel exists} \\ \text{hole} & \text{o.w.} \end{cases} \quad (1)$$

where the weights  $1-v$  and  $v$  are inversely proportional to the virtual view's distance from view 0 and 1. A chosen inpainting algorithm like [11], [12] is then applied to fill in a small number of hole pixels that have no correspondence in both views 0 and 1. In other words, weighted blending is performed if two correspondences are found, while single-pixel mapping and inpainting are invoked if one or zero correspondence is found, respectively. See [7] for details of a standard DIBR view synthesis implementation.

A corresponding pixel  $(i, j^0)$  in the left texture map  $X_t^0$  is a pixel that, given associated disparity  $Y_t^0(i, j^0)$  between left and right views subject to normalization, shifts horizontally by  $Y_t^0(i, j^0) * v * \eta$  pixels to synthesized pixel of coordinate  $(i, j)$  in virtual view  $S_t^v$ , where  $\eta$  is a scaling factor determined by the distance between the capturing cameras. We can write  $j^0$  and  $j^1$  for the two corresponding pixels in left and right texture maps as:

$$\begin{aligned} j &= j^0 - Y_t^0(i, j^0) * v * \eta \\ j &= j^1 + Y_t^1(i, j^1) * (1-v) * \eta \end{aligned} \quad (2)$$

One interpretation of (1) is that the same physical point in the 3D scene (called *voxel* in computer graphics literature [51]) has observed intensities  $X_t^0(i, j^0)$  and  $X_t^1(i, j^1)$  from views 0 and 1, respectively. Hence, the intensity of the same voxel at an intermediate view can be modeled as a convex combination of the two corresponding values. If the surface of the observed physical object has *Lambertian reflectance* [51], then a voxel will have (roughly) the same intensity from different viewpoints; i.e.,  $X_t^0(i, j^0) \approx X_t^1(i, j^1)$ . In such case of *redundant representation* (same intensity value is recorded in two corresponding coordinates at left and right maps), synthesized pixel  $S_t^v(i, j)$  can be perfectly reconstructed even if one of the two corresponding pixels,  $X_t^0(i, j^0)$  and  $X_t^1(i, j^1)$ , is corrupted by channel noise, assuming the decoder knows which corresponding pixel is erred. Based on this observation, and assuming that the majority of synthesized pixels are of

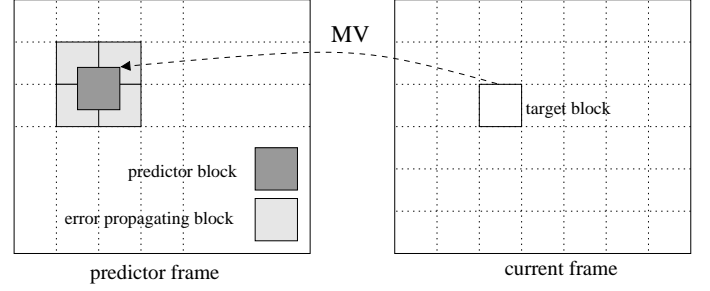


Fig. 2. Motion prediction in differentially coded video causes error propagations from predictor block to target block.

objects with Lambertian reflectance surfaces<sup>3</sup>, we develop the following error concealment strategy during view synthesis.

The key idea of the error concealment strategy for DIBR view synthesis is as follows. When there are two corresponding pixels  $X_t^0(i, j^0)$  and  $X_t^1(i, j^1)$  for a given synthesized pixel  $S_t^v(i, j)$ , decoder can choose to *reweigh* the combination of the pixels depending on the reliability of the two reconstructed pixels. For example, decoder can use only one corresponding pixel for synthesis if the other corresponding pixel is deemed totally unreliable. We next discuss how we estimate the reliability of the two corresponding texture pixels  $X_t^0(i, j^0)$  and  $X_t^1(i, j^1)$  at decoder given observed packet losses in the transmitted maps.

### B. Estimating Texture Error at Decoder

We first compute the reliability of the two corresponding texture pixels  $X_t^0(i, j^0)$  and  $X_t^1(i, j^1)$ , assuming the corresponding disparity pixels  $Y_t^0(i, j^0)$  and  $Y_t^1(i, j^1)$  are correct. Let  $m = b(i, j^0)$  be the MB that contains texture pixel  $(i, j^0)$ , and let  $e_{t,m}$  be the texture error due to packet losses in MB  $m$  given differential coding of texture maps. Depending on whether MB  $m$  is received correctly or not,  $e_{t,m}$  will result in error  $e_{t,m}^+$  and  $e_{t,m}^-$ , respectively:

$$e_{t,m} = \begin{cases} e_{t,m}^+ & \text{if MB } m \text{ is correctly received} \\ e_{t,m}^- & \text{o.w.} \end{cases} \quad (3)$$

Consider first  $e_{t,m}^+$ . If MB  $m$  is an intra-coded block (independently coded) and is correctly received at decoder, then  $e_{t,m}^+ = 0$ . If MB  $m$  is an inter-coded block (differentially coded using a block of a previous frame as predictor) pointing to a previous frame  $\tau_{t,m}$  with motion vector (MV)  $v_{t,m}$ , then  $e_{t,m}^+$  depends on the errors of predictor block in frame  $\tau_{t,m}$ . Note that because the predictor block indicated by MV  $v_{t,m}$  can be located among several coded MBs in frame  $\tau_{t,m}$ , there are typically multiple *error propagating* MBs,  $k \in v_{t,m}$ , that can potentially contribute to  $e_{t,m}^+$ . See Fig. 2 for an illustration.

<sup>3</sup>While common objects like glass and mirrors do not have Lambertian surfaces, if the two captured viewpoints are sufficiently close, voxels of these objects can nonetheless be approximated as having the same intensity values from different but nearby viewpoints.

Thus we write  $e_{t,m}^+$  recursively as follows<sup>4</sup>:

$$e_{t,m}^+(\tau_{t,m}, v_{t,m}) = \begin{cases} 0 & \text{if MB } m \text{ is intra} \\ \gamma \sum_{k \in v_{t,m}} \alpha_k e_{\tau_{t,m},k} & \text{o.w.} \end{cases} \quad (4)$$

where  $\alpha_k$ 's are the weights for the summation in (4) based on the amount of pixel overlaps between the designated predictor block and the error propagating MBs, and  $\gamma < 1$  is the attenuation factor that reflects the dissipating effect of error in an earlier frame over a sequence of motion-compensated frames. In our simulations,  $\gamma$  is chosen to be 0.9.

If MB  $m$  of frame  $t$  is not correctly received, then we assume the decoder performs a block copy from the same MB  $m$  from previous frame  $t-1$ . The resulting error is then error  $e_{t-1,m}$  of MB  $m$  in frame  $t-1$ , plus  $\delta$ , which is the change in intensity between MBs  $m$  in frame  $t-1$  and  $t$ :

$$e_{t,m}^- = e_{t-1,m} + \delta \quad (5)$$

$\delta$  can be estimated at decoder as follows. If there is a corresponding block in texture map of the other captured viewpoint that is more reliably received, then this block is projected onto the current view and  $\delta$  is approximated as the difference between the projected block and the co-located block within the previous frame of the current view. If there is no corresponding block in the other view or the corresponding block is also erred, then we estimate  $\delta$  as the difference among co-located blocks of the previous two frames within the current view. For the initial frames in which one or two previous frames are not available,  $\delta$  is estimated from spatially neighboring blocks with similar disparity values (i.e., of similar depth and hence likely the same physical object).

### C. Estimating Disparity Error at Decoder

Similarly, we can compute the error in left disparity pixel  $Y_t^0(i, j^0)$  (or right disparity pixel  $Y_t^1(i, j^1)$ ) by estimating the error in the MB  $m = (i, j^0)$  (or  $m = (i, j^1)$  for right disparity pixel) that contains it. We can estimate the disparity error<sup>5</sup>  $\epsilon_{t,m}$  in MB  $m$  using recursion as done for  $e_{t,m}$  in (3). In this case, derivation of disparity errors due to correctly received and lost MBs are analogous to the presented in (4) and (5), respectively, with the exception that  $\delta$  is always estimated from co-located blocks within the previous two frames.

The effect of a disparity error on the synthesized pixel  $(i, j)$ , however, is more indirect; a disparity error causes the wrong corresponding pixel  $X_t^0(i, j^\#)$  to be used for synthesis of pixel  $(i, j)$  in virtual view  $S_t^v$ . Now if the pixel patch around the local neighborhood of texture pixel  $X_t^0(i, j^0)$  is monotone, then using a texture pixel from a slightly off location  $(i, j^\#)$  will result in very small increase in synthesized distortion. On the other hand, if the patch around texture pixel  $(i, j^0)$  has high texture variation, then the resulting synthesized distortion can be significant.

<sup>4</sup>Though we have already argued that inter-view prediction is not a sensible coding option for our loss-resilient free viewpoint video streaming framework, (4) can nonetheless be modified easily to account for inter-view dependencies if deployed.

<sup>5</sup>If a depth block is predicted from the corresponding texture block of the same view as done in [29], (4) can be easily modified accordingly to reflect the inter-component dependency.

### D. Proposed View Synthesis

Having computed the estimated texture error  $e_{t,m}$  and disparity error  $\epsilon_{t,m}$  for the two MBs  $m$  that contain corresponding texture pixel  $X_t^0(i, j^0)$  and depth pixel  $Y_t^0(i, j^0)$  of the left view respectively, as described in the past two sections, we now derive the *worst case distortion*  $d^0(i, j^0)$  for left corresponding pixel  $X_t^0(i, j^0)$ . Then, left reliability term  $r^0$  can be subsequently computed. Together with right reliability term  $r^1$ , they determine how the two corresponding texture pixels  $X_t^0(i, j^0)$  and  $X_t^1(i, j^1)$  should be reweighed for our adaptive, error-aware pixel blending.

Because disparity error leads to the selection of a wrong texture pixel for blending, given the estimated disparity error  $\epsilon_{t,m}$ , we will consider the possible adverse effect of using texture pixel  $X_t^0(i, l)$  for synthesis instead of  $X_t^0(i, j^0)$ , where  $l$  in the range  $[j^0 - \epsilon_{t,m}, j^0 + \epsilon_{t,m}]$ . Specifically, for each texture pixel  $X_t^0(i, l)$ , we consider both the pixel-to-pixel texture intensity difference  $|X_t^0(i, l) - X_t^0(i, j^0)|$  and the estimated texture error due to channel losses  $e_{t,b(i,l)}$  for texture pixel  $X_t^0(i, l)$ . Mathematically, the worst-case distortion  $d^0(i, j^0)$  for texture pixel  $X_t^0(i, j^0)$  considering all pixels  $(i, l)$  in the range is computed as follows:

$$d^0(i, j^0) = \max_{l=j^0-\epsilon_{t,m}, \dots, j^0+\epsilon_{t,m}} \{e_{t,b(i,l)} + |X_t^0(i, l) - X_t^0(i, j^0)|\} \quad (6)$$

As done for  $\delta$ , the pixel intensity difference  $|X_t^0(i, l) - X_t^0(i, j^0)|$  in (6) can be estimated at decoder using either corresponding pixels in texture map of the other captured view that is more reliably received, or MBs of previous correctly received frames of the same view with similar disparity values.

Having derived worst case distortion  $d^0(i, j^0)$  and  $d^1(i, j^0)$  for texture pixels,  $X_t^0(i, j^0)$  and  $X_t^1(i, j^1)$ , we now define a reliability metric,  $r^0$  and  $r^1$ , inversely proportional to distortion for the two pixels as follows:

$$r^0 = w \left( \frac{\kappa}{d^0(i, j^0) + \kappa} \right). \quad (7)$$

In our implementation,  $\kappa = d^1(i, j^0) + c$  such that distortion from both views are taken into consideration.  $c$  is a small positive constant chosen so that  $r^0$  is well defined even if both distortions are zero and  $w$  is a scaling factor so that  $r^0 + r^1 = 1$ .

## V. BLOCK-LEVEL REFERENCE PICTURE SELECTION

Having described the error concealment strategy deployed during view synthesis at the receiver, we now turn our attention to optimization at the sender. At the sender side, during real-time encoding of both texture and depth maps, the encoder has the flexibility to select any MB in any past coded frame for motion compensation (MC) to encode each MB in a current frame  $t$ . Using a well matched MB from the immediate previous frame  $t-1$  for MC would lead to small encoding rate, but may result in large expected distortion at receiver due to a possibly long dependency chain of differentially coded MBs. Using a MB from a frame further into the past for MC (or an intra-coded MB), will lead to a larger encoding rate, but

will also result in a smaller expected distortion. Exploiting this flexibility of *reference picture selection* (RPS), the goal is to pro-actively minimize the overall expected distortion of an intermediate view at instant  $t$ , synthesized via DIBR using texture and depth maps of two adjacent coded views at decoder as described in the previous section, and subject to a transmission rate constraint. Leveraging our derivation for estimated texture and disparity errors at the receiver in the previous section, we first discuss how synthesized distortion in an interpolated view is estimated at the sender. We then present the mathematical formulation of our proactive-feedback block-level RPS optimization.

#### A. Estimating Texture & Disparity Error at Sender

We first estimate the expected texture error  $e_{t,m}$  of a MB  $m$  in frame  $t$  at sender in differentially coded texture video as follows. Let  $e_{t,m}(\tau_{t,m}, v_{t,m})$  be the texture error given it is motion-compensated using a block identified by MV  $v_{t,m}$  inside a previous transmitted frame  $X_{\tau_{t,m}}$ ,  $\tau_{t,m} < t$ . Let  $p$  be the probability that MB  $m$  is correctly *received*. Similar to (3), we can write  $e_{t,m}(\tau_{t,m}, v_{t,m})$  in terms of  $e_{t,m}^+(\tau_{t,m}, v_{t,m})$  and  $e_{t,m}^-(\tau_{t,m}, v_{t,m})$ , the expected texture error of MB  $m$  if it is correctly received and lost, respectively. Unlike (3), the expression is now probabilistic and depends on  $p$ , because the delivery status of packet that contains MB  $m$  is not known at sender before it is transmitted:

$$e_{t,m}(\tau_{t,m}, v_{t,m}) = p e_{t,m}^+(\tau_{t,m}, v_{t,m}) + (1 - p) e_{t,m}^- \quad (8)$$

$e_{t,m}^+(\tau_{t,m}, v_{t,m})$  and  $e_{t,m}^-$  can be computed recursively using previously derived (4) and (5), respectively. In this case,  $\delta$  is the difference between the current block and the co-located in the previous frame. Expected disparity error  $\epsilon_{t,m}(\rho_{t,m}, u_{t,m})$  given MV  $u_{t,m}$  in previous disparity frame  $Y_{\rho_{t,m}}$  can be computed in a similar fashion.

#### B. Computing Expected Synthesized View Distortion at Encoder

Having derived expected texture and disparity errors  $e_{t,m}^0$  and  $\epsilon_{t,m}^0$  for a given MB  $m$  in texture and disparity frames  $X_t^0$  and  $Y_t^0$  of view 0, we now analyze the adverse effects of these errors to expected distortion in the synthesized image  $S_t^v$  of virtual view  $v$  at receiver. One way to compute the expected synthesized distortion is to use a similar distortion expression as one derived in (6) for receiver that ties both error terms together in a non-trivial way. However, this will introduce inter-dependency among MBs in texture and depth maps, which will render the subsequent block-level RPS optimization very difficult.

Instead, we will use the following simplification. Texture error  $e_{t,m}^0$ , as discussed in Section IV-B, contributes directly to the synthesized distortion. To estimate the ill effects of disparity error  $\epsilon_{t,m}^0$  to synthesized distortion, we model synthesized distortion as a quadratic function  $g_{t,m}^0(\cdot)$  of disparity error  $\epsilon_{t,m}^0$ :

$$g_{t,m}^0(\epsilon_{t,m}^0) = \frac{1}{2} a_{t,m}^0 (\epsilon_{t,m}^0)^2 \quad (9)$$

where  $a_{t,m}^0$  is the single parameter that describes the curvature of the quadratic function  $g_{t,m}^0(\epsilon_{t,m}^0)$ .

This quadratic modeling of synthesized distortion was first used in [27] for depth map coding. The key idea in the model is to capture the synthesized view distortion sensitivity to disparity error in MB  $m$  in a single parameter  $a_{t,m}^0$ . Specifically, we perform the following procedure for each disparity pixel in the block. We first construct a true synthesized distortion function for each pixel describing the resulting distortion as disparity value deviates from the ground truth value. Then, we identify the nearest *boundary disparity values* below and above the ground truth where the corresponding synthesized distortion exceed a pre-defined threshold. Using ground truth and each of boundary disparity values, one can construct two quadratic functions, or parabolas, with slope zero at ground truth. The curvature of the sharper of the two parabolas is then chosen, and parameter  $a_{t,m}^0$  in (9) is the average of all chosen curvatures of pixels in the block. See Fig. 3 for an example and [27] for more details.

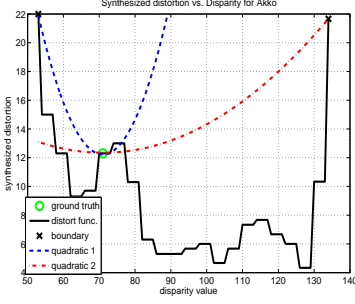
In general, if the textural area corresponding to the depth MB  $m$  is smooth and inside a physical object, then synthesized distortion will not be sensitive to disparity error. The reason is that small error  $\epsilon_{t,m}^0$  leading to mapping of wrong texture pixels of similar intensities in the local neighborhood will result in only small synthesized distortion. On the other hand, if the textural area corresponding to the depth MB  $m$  has large frequency contents inside a physical object or contains boundary pixels between foreground object and the background, then synthesized distortion will be sensitive to disparity error.

1) *Computing block curvature  $a_{t,m}^0$* : Specifically, we compute parameter  $a_{t,m}^0$  for each MB  $m$  as follows. Distortion  $d_{t,m}^0$  of MB  $m$  is computed as a sum of its constituent pixels  $(i, j)$ 's distortions. As discussed in Section IV-A, a texture pixel  $X_t^0(i, j)$  in the left texture map can be mapped to a shifted pixel  $X_t^1(i, j - Y_t^0(i, j) * \eta)$  in the right texture map. We thus express synthesized distortion  $d_{t,m}^0(\epsilon_{t,m}^0)$  of MB  $m$  as the sum of the differences in texture pixel values between left pixels  $X_t^0(i, j)$ 's and mapped right pixels  $X_t^1(i, j - (Y_t^0(i, j) + \epsilon_{t,m}^0) * \eta)$ 's due to disparity error  $\epsilon_{t,m}^0$ :

$$d_{t,m}^0(\epsilon_{t,m}^0) = \sum_{(i,j) \in MB_m} |X_t^0(i, j) - X_t^1(i, j - (Y_t^0(i, j) + \epsilon_{t,m}^0) * \eta)| \quad (10)$$

The synthesized distortion function  $d_{t,m}^0(\epsilon_{t,m}^0)$  for a pixel of view 47 of the multiview image sequence Akko and Kayo [52] is shown in black in Fig. 3(a). We see that as the disparity error  $\epsilon_{t,m}^0$  increases, i.e., the depth value moves away from ground truth, the distortion also increases generally. Our model  $g_{t,m}^0(\epsilon_{t,m}^0)$  will simply be the sharpest of the two quadratic functions fit to  $d_{t,m}^0(\epsilon_{t,m}^0)$  as illustrated in Fig. 3(a). As an example, in Fig. 3(b) and (c), the original frame from view 47 of Akko and Kayo and the per-pixel curvatures of the quadratic model functions of the corresponding depth map are shown. We can clearly see that larger curvatures (in white) occur at object boundaries, agreeing with our intuition that a synthesized view is more sensitive to depth pixels at object boundaries.





(a) Synthesized distortion functions



(b) original frame



(c) Per-pixel curvatures

Fig. 3. Synthesized distortion and quadratic model functions for one pixel are shown in (a) for image Akko and Kayo view 47 in (b). The resulting curvatures for entire image are shown in (c).

Combining synthesized distortion due to disparity error  $\epsilon_{t,m}^0$  with that of texture error  $e_{t,m}^0$ , we can write the block-level RPS optimization for MB  $m$  in texture and depth maps of view 0 as:

$$\min_{\tau_{t,m}^0, v_{t,m}^0, \rho_{t,m}^0, u_{t,m}^0} \bar{D}_{t,m}^0(\tau_{t,m}^0, v_{t,m}^0, \rho_{t,m}^0, u_{t,m}^0) = e_{t,m}^0(\tau_{t,m}^0, v_{t,m}^0) + g_{t,m}^0(\epsilon_{t,m}^0(\rho_{t,m}^0, u_{t,m}^0)) \quad (11)$$

where  $\bar{D}_{t,m}^0$  denotes the expected distortion for a MB in frame  $t$ . In words, (11) says that the expected distortion for MB  $m$  is a simple sum of: i) expected texture error  $e_{t,m}^0$ , and ii) a quadratic term of the expected disparity error  $\epsilon_{t,m}^0$ . This simple linear model for distortion will play a significant role in simplifying the to-be-discussed RPS optimization procedure.

2) *Consideration for Receiver's Error Concealment:* Because of the error concealment scheme performed at decoder for MBs that are visible from both captured views, as discussed in the previous section, distortion due to errors in MB  $m$  of frames  $X_t^0$  and  $Y_t^0$  in view 0 will contribute to the actual synthesized view distortion *only if* errors in the corresponding pixels in frames  $X_t^1$  and  $Y_t^1$  of view 1 are worse. Otherwise, pixels in  $X_t^1$  and  $Y_t^1$  will be reweighted more heavily in the view synthesis process. Given the above observation, we can rewrite the expected synthesized view distortion  $D_{t,m}^0$  in (11) due to texture and depth errors in MB  $m$  of texture and depth frames  $t$  of view 0, as:

$$D_{t,m}^0(\tau_{t,m}^0, v_{t,m}^0, \rho_{t,m}^0, u_{t,m}^0) = \min \{ e_{t,m}^0(\tau_{t,m}^0, v_{t,m}^0) + g_{t,m}^0(\epsilon_{t,m}^0(\rho_{t,m}^0, u_{t,m}^0)), \max_{k \in S_m^1} [e_{t-1,k}^1 + g_{t-1,k}^1(\epsilon_{t-1,k}^1) + \delta] \} \quad (12)$$

where  $S_m^1$  is the set of MBs in view 1 that contains pixels corresponding to MB  $m$  in view 0. In words, (12) states that the synthesized distortion due to errors in MB  $m$  of view 0 is the smaller of distortion due to view 0 and distortion due to view 1. Note that we write distortion due to view 1 using errors in *previous frames*  $X_{t-1}^1$  and  $Y_{t-1}^1$  plus  $\delta$ , so that  $D_{t,m}^0$  will not have dependency on MVs of current frames  $X_t^1$  and  $Y_t^1$  of view 1. (Recall  $\delta$  is the change in intensity between MBs in frame  $t-1$  and  $t$ .) This avoids inter-dependency

of free variables, simplifying the to-be-discussed optimization algorithm.

### C. Block-level Reference Picture Optimization

We are now ready to formally define our optimization for block-level reference picture selection. Our objective is to minimize the sum of induced synthesized distortion from MB  $m$  in both view 0 and 1:

$$\min_{\{\tau_{t,m}^i, v_{t,m}^i, \rho_{t,m}^i, u_{t,m}^i\}} \sum_{i \in \{0,1\}} \left( \sum_{m \in \bar{\mathcal{L}}_t} \bar{D}_{t,m}^i(\tau_{t,m}^i, v_{t,m}^i, \rho_{t,m}^i, u_{t,m}^i) + \sum_{m \in \mathcal{L}_t} D_{t,m}^i(\tau_{t,m}^i, v_{t,m}^i, \rho_{t,m}^i, u_{t,m}^i) \right) \quad (13)$$

where  $\bar{\mathcal{L}}_t$  and  $\mathcal{L}_t$  are the set of MBs in frame  $t$  without and with corresponding MBs in the opposing captured view, respectively.

We note that (13) is an approximation of the actual synthesized distortion at intermediate view  $S_t^v$ . Nonetheless, (13) is a good approximation when only one of the two errors  $e_{t,m}^i$  and  $\epsilon_{t,m}^i$  is non-zero, and it leads to a simple optimization procedure as discussed in Section V-D.

The optimization is subject to the rate constraint  $R_t$  at instant  $t$ :

$$\sum_{i \in \{0,1\}} \sum_m r_{t,m}^i(\tau_{t,m}^i, v_{t,m}^i) + \zeta_{t,m}^i(\rho_{t,m}^i, u_{t,m}^i) \leq R_t \quad (14)$$

where  $r_{t,m}^i$  and  $\zeta_{t,m}^i$  are the resulting bit overhead required to code MB  $m$  in texture and depth frame of view  $i$ ,  $X_t^i$  and  $Y_t^i$ , respectively, given selection of reference frame / MV pair,  $(\tau_{t,m}^i, v_{t,m}^i)$  and  $(\rho_{t,m}^i, u_{t,m}^i)$ , respectively.

### D. Optimization Algorithm

Instead of solving the constrained optimization problem (13) and (14), we can solve the corresponding Lagrangian problem instead for given multiplier  $\lambda > 0$ :



$$\begin{aligned}
& \min_{\{\tau_{t,m}^i, v_{t,m}^i, \rho_{t,m}^i, u_{t,m}^i\}} \sum_{i \in \{0,1\}} \left( \sum_{m \in \mathcal{L}_t} \bar{D}_{t,m}^i(\tau_{t,m}^i, v_{t,m}^i, \rho_{t,m}^i, u_{t,m}^i) \right. \\
& \quad + \sum_{m \in \mathcal{L}_t} D_{t,m}^i(\tau_{t,m}^i, v_{t,m}^i, \rho_{t,m}^i, u_{t,m}^i) \left. \right) \\
& \quad + \lambda \sum_{i \in \{0,1\}} \sum_m (r_{t,m}^i(\tau_{t,m}^i, v_{t,m}^i) \\
& \quad + \zeta_{t,m}^i(\rho_{t,m}^i, u_{t,m}^i)) \quad (15)
\end{aligned}$$

To solve (15) optimally, it is clear that we can separately optimize each pair of MBs  $m$  in texture and disparity frame  $X_t^i$  and  $Y_t^i$ . For MB  $m$  that has no corresponding MB in opposing view, i.e.,  $m \in \bar{\mathcal{L}}_t$ :

$$\begin{aligned}
& \min_{\tau_{t,m}^i, v_{t,m}^i, \rho_{t,m}^i, u_{t,m}^i} \bar{D}_{t,m}^i(\tau_{t,m}^i, v_{t,m}^i, \rho_{t,m}^i, u_{t,m}^i) \\
& + \lambda [r_{t,m}^i(\tau_{t,m}^i, v_{t,m}^i) + \zeta_{t,m}^i(\rho_{t,m}^i, u_{t,m}^i)] \quad \forall i, m \quad (16)
\end{aligned}$$

In this case,  $\bar{D}_{t,m}^i$  separates into two terms,  $e_{t,m}^i$  and  $g_{t,m}^i$ , and the texture and depth map MB variables can clearly be optimized separately.

For MB  $m$  that has a corresponding MB in opposing view,  $\bar{D}_{t,m}^i$  is replaced by  $D_{t,m}^i$  in (16). There is now an interdependency between texture and depth map MB variables in the distortion term. We can simplify (16) into the following two equations, where  $(\tau_{t,m}^{i,*}, v_{t,m}^{i,*})$  means the best MV that minimizes texture error  $e_{t,m}^i$  only, so that the searches for MV for texture and depth maps can be performed separately:

$$\begin{aligned}
& \min_{\tau_{t,m}^i, v_{t,m}^i} D_{t,m}^i(\tau_{t,m}^i, v_{t,m}^i, \rho_{t,m}^{i,*}, u_{t,m}^{i,*}) + \lambda r_{t,m}^i(\tau_{t,m}^i, v_{t,m}^i) \quad \forall i, m \\
& \min_{\rho_{t,m}^i, u_{t,m}^i} D_{t,m}^i(\tau_{t,m}^{i,*}, v_{t,m}^{i,*}, \rho_{t,m}^i, u_{t,m}^i) + \lambda \zeta_{t,m}^i(\rho_{t,m}^i, u_{t,m}^i) \quad \forall i, m \quad (17)
\end{aligned}$$

Equation (17) is an approximation to (16) in the following sense. If errors in the opposing views in (12) are relatively large, then errors  $e_{t,m}^i$  and  $\epsilon_{t,m}^i$  can indeed be separately optimally traded off with their respective rate terms  $r_{t,m}^i$  and  $\zeta_{t,m}^i$ , as done in (17), with no loss in optimality. If errors in the opposing views are relatively small, then errors in current view can actually be ignored. Hence by setting MV of texture map to be best error-minimizing one  $(\tau_{t,m}^{i,*}, v_{t,m}^{i,*})$  when optimizing MV of disparity map, we are forcing the optimization to focus on minimizing induced synthesized distortion unless errors in opposing views are very small comparatively. This conservative approach ensures the combined resulting induced synthesized distortion from texture and disparity errors will not be large. (17) is minimized by searching through all feasible MVs in all valid reference frames. This can be done efficiently, for example, in a parallel implementation.

## VI. COMPLEXITY ANALYSIS

The proposed strategies introduce additional complexity costs for both the sender and receiver of the free-viewpoint conferencing system. At the sender side, the proposal with largest computational load is the determination of the curvature

parameters representing sensitivity to disparity errors employed in (9). Though in our current implementation we compute  $a_{t,m}^0$  for block  $m$  in (9) by first painstakingly computing curvature parameters for each pixel in the block as described in Section V-B, one can approximate  $a_{t,m}^0$  in a computation-efficient manner by simply examining the high frequency DCT components of block  $m$  and its neighboring blocks in texture and depth maps (high frequencies in depth block indicate an edge, while high frequencies in texture block indicate fast changing textural content.) As fast curvature parameter approximation is not the main focus of this paper, we simply assume curvature parameters can be computed efficiently and discuss complexity of our proposed optimization procedures.

Still at sender, the loss-resilient coding proposals encompass the estimation of texture/disparity errors and the optimization of RPS. Texture error estimation involves determining  $e^+$  and  $e^-$  as combined in (8) and defined by (4) and (5), respectively. When correctly received,  $e^+$  of a non-intra MB of size  $N \times N$  involves a weighted average over all the MB pixels and thus  $N \times N$  multiplication operations. The error  $e^-$  of an incorrectly received MB is a function of  $\delta$  which is taken as the difference between the current MB and the co-located MB of the previous frame. This difference contributes in  $N \times N$  subtraction operations to the complexity count. Complexity analysis of disparity error estimation for encoding provides similar results. Lastly, the optimization algorithm, described in sub-section V-D, considers the tradeoff between an expected distortion measure comprised of texture and disparity errors across both views and rate terms for selecting reference pictures. It is used in substitution of the standard rate-distortion optimization employed in coding of texture and depth and thus imposes no additional computational complexity costs. The aforementioned coding proposals represent a modest complexity increment in terms of arithmetic operations. In our implementation, an average increase of only 1.6% in execution time with respect to coding with reactive feedback channel was registered. Note that for these simulations fast motion estimation was used and file I/O operations, used in our implementation, were not considered.

At the receiver, texture and disparity error estimation for decoding present a computational cost similar to the one determined for the sender. Nonetheless, when decoding, the estimation of  $\delta$  in (5) is dependent on whether packets of both views are lost simultaneously or whether packets in only one view are lost. In the former case, delta is the difference among co-located MBs in the two previous frames, representing  $N \times N$  subtraction operations. In the latter case, prior to estimating  $\delta$  as a difference of MBs, the correctly received pixels from the adjacent view are projected onto the view with losses, representing an extra  $N \times N$  addition operations. Furthermore, at the receiver, the worst case distortion defined in (6) must be calculated for the virtual view prior to adaptive blending. This calculation represents  $N \times N \times (2\epsilon_{t,m} + 1)$  subtraction operations. Here, the disparity error  $\epsilon_{t,m}$  is content dependent and generally small except along boundary pixels with large intensity differences. The adaptive blending step, based on worst case distortion estimates, is equivalent in complexity to the standard blending procedure which it sub-

stitutes. In conclusion, our decoding proposals also impose a modest complexity increment in terms of additional arithmetic operations.

## VII. EXPERIMENTATION

We verify the contributions of our proposed error-concealment strategy during view synthesis (adaptive blending) as well as our proposed block-level RPS encoding strategy (proactive-feedback) through extensive experiments in this section. We first describe the experimental setup in which our proposals are compared, and then present streaming results in terms of an objective measure (PSNR) and subjective gains.

### A. Experimental Setup

Our proposed view synthesis strategy, as described in Section IV, is based on an error-aware *adaptive blending* procedure. Adaptive blending is implemented in the MPEG View Synthesis Reference Software (VRS v3.5) [6] and comparisons are drawn against the standard version of the software.

In addition to evaluating the contributions of adaptive blending, the proposed proactive-feedback RPS encoding strategy is compared to two other RPS-based error-resilient alternatives. Note that in all RPS strategies we assume a feedback channel is present. The channel can transmit acknowledgment to the encoder, after a round-trip-time delay (RTT), of whether a packet has been correctly received or lost. In our experiments, RTT is set to be constant and fixed to 133 ms (4 frame of delay at 30 fps).

The first RPS alternative reacts to feedback information by avoiding the use of loss-affected regions in past frames as reference for coding of future MBs. This alternative is termed *reactive feedback* and serves as a baseline for comparisons. The second RPS alternative employed in our tests is based on our previous work [31]. Similar to our current proposal, [31] consists of a proactive RPS scheme combined with feedback information, which estimates the reconstructed error of a block from given past frames, protecting those of greater importance to synthesis. However, unlike our current proposal, in [31] views are encoded independently, *i.e.*, expected distortions of one view do not affect the encoding of the adjacent view. Note that the experimental results reported in [31] used a different feedback channel which only acknowledged whether an entire frame was received error-free.

From the described view synthesis and RPS encoding strategies, four setups are tested in the following sections:

- standard blending with reactive feedback channel (RFC),
- standard blending with proactive RPS from [31] with feedback information (RPS1),
- standard blending with the proposed proactive RPS with feedback information (RPS2) and
- the proposed adaptive blending with the proposed proactive RPS with feedback information (ARPS).

All results are evaluated in terms of synthesized view quality. Specifically, for each multi-view sequence, we choose three neighboring views, and transmit only the left and right views, reserving the withheld center view as ground truth.

We use test sequences from the Nagoya University database [52]. The selected sequences are the first 150 frames of: Pantomime ( $1280 \times 960$  pixels), Kendo ( $1024 \times 768$  pixels) and Akko and Kayo ( $640 \times 480$  pixels), all at 30 fps. For Pantomime view 40 was synthesized using views 39 and 41, for Kendo view 2 is interpolated from view 1 and 3, and for Akko and Kayo views 47 and 49 are used to synthesize view 48. The view synthesis software [6] was set to work with integer pixel precision.

Currently, our encoding scheme, including error estimation, is implemented only for  $P16 \times 16$  mode in H.264/AVC JM reference software v18.0 [53]. Therefore, the only modes available in all simulations are  $P16 \times 16$ , Skip or Intra blocks (no block or sub-block partitions are allowed). More extensive comparison using larger number of available modes is a subject of future study. Note that the appropriate  $\lambda$  for (17) in all simulations was selected empirically. The QP was set to 28 in all setups.

Four transport packets are used for each depth map frame, while twelve are used for each texture frame packets due to higher associated bit rates. Simulations include losses of 2%, 5% and 8% of the packets for both texture and depth maps. In order to provide meaningful comparisons, the same packets are lost in all schemes. We assume the picture parameter set (PPS) and sequence parameter set (SPS) are reliably transmitted out-of-band. Both depth maps and texture are encoded using 64 pixel search window, CABAC entropy encoder and *IPPP...* encoding mode. When a MB is lost during transmission, the co-located block from the previous frame is used in its place.

### B. Objective Streaming Performance

In this subsection we present the results of our simulations using PSNR as an objective quality metric. The bitrates for each sequence, for each percentage of lost packets, are presented in Table I. The bitrates are computed considering both views and depth maps. Note that, as defined by (8), the probability of MB losses is considered during error estimation. Therefore, as this probability increases, the encoder raises the level of protection in each MB resulting in higher bitrates as seen in Table I. The most suitable  $\lambda$  in (17) can be found via binary search where the optimization problem is solved multiple times (each time with a different  $\lambda$ ) for each frame. In practice, the  $\lambda$  that is used in previous frame can be reused, with an optional local adjustment if the resulting rate is too far below or above a rate constraint. In our experiments, we first run the RFC setup. Then, we select among various tested candidates the  $\lambda$  for RPS1 and RPS2 which results in bitrate closest to that of RFC. Our goal was to match the bitrates between all setups in order to make a fair comparison between them.

A summary of the PSNR results obtained for synthesized views (assuming original views as ground truth) can be found in Tables II and III. Table II presents the average PSNR over all frames for each sequence and error rate for all four tested setups: *RFC*, *RPS1*, *RPS2* and *ARPS*. Table III shows the maximum PSNR gain for a single frame in each simulation when comparing setups RPS1, RPS2 and ARPS to the use of RFC.

TABLE I  
BITRATES USED DURING SIMULATIONS (INCLUDING BOTH VIEWS AND DEPTH MAPS)

Sequence	Loss Rate	Bitrate
Pantomime	2%	9.7 Mbps
	5%	10.2 Mbps
	8%	11.2 Mbps
Kendo	2%	6.7 Mbps
	5%	6.8 Mbps
	8%	7.0 Mbps
Akko and Kayo	2%	6.6 Mbps
	5%	7.0 Mbps
	8%	7.5 Mbps

TABLE II  
AVERAGE PSNR OVER ALL FRAMES FOR TESTED SETUPS.

Sequence	Loss Rate	Avg. PSNR			
		RFC	RPS1	RPS2	ARPS
Pantomime	2%	31.44 dB	31.65 dB	31.70 dB	31.81 dB
	5%	30.02 dB	30.33 dB	30.44 dB	30.62 dB
	8%	28.99 dB	29.41 dB	29.47 dB	29.68 dB
Kendo	2%	33.41 dB	33.59 dB	33.62 dB	33.74 dB
	5%	31.79 dB	32.23 dB	32.32 dB	32.45 dB
	8%	30.37 dB	30.85 dB	31.00 dB	31.19 dB
Akko and Kayo	2%	28.08 dB	28.15 dB	28.19 dB	28.22 dB
	5%	26.85 dB	26.97 dB	27.03 dB	27.06 dB
	8%	26.16 dB	26.37 dB	26.44 dB	26.53 dB

We first observe that results RPS1, based on previous work [31], already outperform the use of RFC. In terms of average PSNR, RPS1 outperforms RFC by as much as 0.48 dB for Kendo at 8% error rate as shown in Table II. For Pantomime and Akko and Kayo the largest average gains are of 0.42 dB and 0.21 dB, respectively. Note that when comparing RPS1 to RFC, the gains increase as the error rates increase for all sequences. For a single frame, shown in Table III, RPS1 can outperform RFC by as much as 2.01 dB

The results obtained by RPS2 show an improvement over previous work RPS1. However, improvements are modest since both schemes use similar optimization processes. The main difference is that the proposed encoding strategy in RPS2 protects each MB simultaneously in both views, therefore the same level of protection is achieved with a smaller bitrate. By combining our proposed encoding with our proposed adaptive blending (ARPS) significant improvements are achieved, specially for Pantomime and Kendo. From Table II, we observe that ARPS can outperform the use of a RFC by as much as 0.82 dB for Kendo at 8% error rate. The maximum gain of ARPS with respect to RFC for a single frame, presented in Table III, is 3.29 dB for Kendo.

In Fig. 4, PSNR values for the proposed ARPS and the baseline RFC are presented for each frame. Both schemes consider a 5% packet loss rate and PSNR values are shown from frame 20 though frame 150 for better visualization. Due to the use of feedback, we see that both schemes are generally able to avoid continuous propagation of errors due to losses. Nevertheless, we see that our method can better withstand the transient effect of packet losses by providing stronger

TABLE III  
MAXIMUM PSNR GAIN FOR A SINGLE FRAME WITH RESPECT TO RFC.

Sequence	Loss Rate	Max. PSNR Gain		
		RPS1	RPS2	ARPS
Pantomime	2%	1.26 dB	1.52 dB	2.00 dB
	5%	0.86 dB	1.01 dB	1.45 dB
	8%	1.13 dB	1.25 dB	1.64 dB
Kendo	2%	1.42 dB	1.48 dB	1.72 dB
	5%	1.69 dB	1.81 dB	2.94 dB
	8%	2.01 dB	2.03 dB	3.29 dB
Akko and Kayo	2%	0.27 dB	0.27 dB	0.31 dB
	5%	0.50 dB	0.55 dB	0.64 dB
	8%	0.47 dB	0.51 dB	0.67 dB

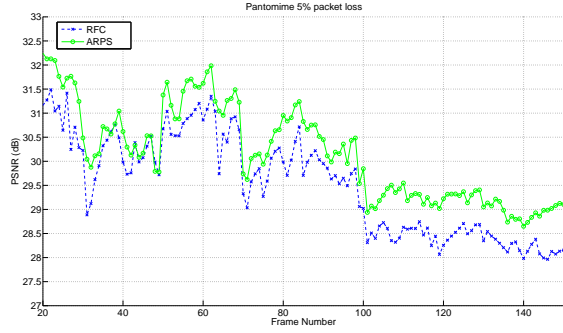
protection to more important regions. Furthermore, our ARPS consistently performs above RFC.

### C. Visual Gains

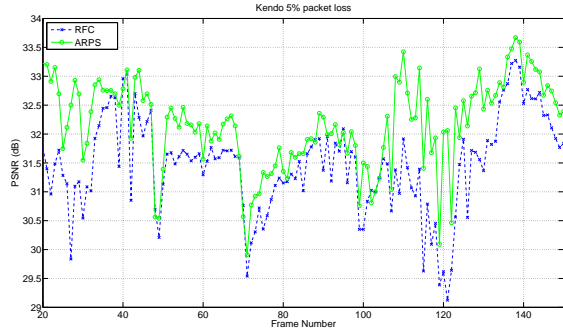
For subjective comparisons, Figs. 5-7 present, for each sequence, synthesized views resulting from the application of methods RFC, RPS1 and ARPS. The more significant differences among images are circled in red. Visual gains between methods are very significant for both the Kendo and Pantomime sequences and they can be easily perceived at normal frame rate 30 fps.

In Kendo, for example, we can see errors in the RFC image (top frame of Fig. 6) around both swords and above the audience. The errors in the background above the audience are residue created by using co-located blocks to conceal errors in past frames, which were not yet acknowledged by the feedback channel. The errors around the swords are most likely caused by packets that were lost in the depth maps, generating an erroneous horizontally shift. The RPS1 scheme reduces the errors in the background and the unequal protection in the depth maps helps to conserve the sharp edges around the swords, which avoids such visual degradations, as can be seen in the middle frame of Fig. 6. The proposed adaptive blending significantly improves the synthesized view by applying weights that consider the estimated error in each pixel. The residue errors above the audience is minimal in the bottom frame of Fig. 6, resulting in a more pleasing subjective viewing. Note that these highly visible difference in visual quality need not give rise to large PSNR difference, as the artifacts affect only a small portion of the image.

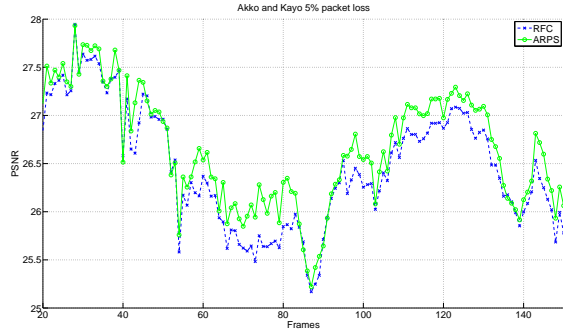
Similar results can be seen in Fig. 5 for Pantomime below the elbow and near the waist of the clown in the left and in the left arm of the clown in the right. For Akko and Kayo the subjective gains are not as significant as in the other two sequences and are harder to perceive by a untrained viewer at regular frame rate. However, it is important to notice that the view synthesis software does not perform as well in this sequence as in the other two, therefore it limits the subjective gains that our adaptive blending can achieve. Nevertheless, the improvement of a particular frame can be significant as shown in Fig. 7.



(a)



(b)



(c)

Fig. 4. PSNR per frame for ARPS and RFC at 5% packet loss rate for (a) Pantomime, (b) Kendo and (c) Akko and Kayo.

## VIII. CONCLUSION

To enable free-viewpoint video conferencing, in this paper we study a real-time streaming system where texture and depth videos from two captured viewpoints are transmitted, so that synthesis and display of any intermediate viewpoint at receiver is enabled via depth-image-based rendering (DIBR). To provide resiliency over loss-prone transmission networks, we propose first to adaptively blend a synthesized pixel at receiver, so that the pixels from the more reliable transmitted view is weighted heavier during synthesis. We then propose a reference picture selection (RPS) scheme at sender, so that pro-actively important code blocks containing pixels vital to synthesized view quality are predicted from older past frames, lowering their expected error due to error propagation in differentially coded video. Finally, we analyze synthesized



(a)



(b)



(c)

Fig. 5. Synthesized views for Pantomime, frame 118, at 5% packet loss. (a) RFC, (b) RPS1 and (c) ARPS schemes.





(a)



(b)



(c)

Fig. 6. Synthesized views for Kendo, frame 22, at 5% packet loss. (a) RFC, (b) RPS1 and (c) ARPS schemes.



(a)



(b)



(c)

Fig. 7. Synthesized views for Akko and Kayo, frame 38, at 5% packet loss. (a) RFC, (b) RPS1 and (c) ARPS schemes.

view distortion sensitivities to texture versus depth errors, so that relative importance can be determined for texture and depth code blocks for system-wide RPS optimization. Experimental results show that our proposed scheme, combined with feedback information, can significantly outperform a reactive feedback channel, not only by objective metrics, but subjectively as well.

## REFERENCES

- [1] A. Kubota, A. Smolic, M. Magnor, M. Tanimoto, T. Chen, and C. Zhang, "Multi-view imaging and 3DTV," in *IEEE Signal Processing Magazine*, vol. 24, no.6, November 2007.
- [2] C. Zhang, Z. Yin, and D. Florencio, "Improving depth perception with motion parallax and its application in teleconferencing," in *IEEE International Workshop on Multimedia Signal Processing*, Rio de Janeiro, Brazil, October 2009.
- [3] T. Fujii, K. Mori, K. Takeda, K. Mase, M. Tanimoto, and Y. Suenaga, "Multipoint measuring system for video and sound—100 camera and microphone system," in *IEEE International Conference on Multimedia and Expo*, Toronto, Canada, July 2006.
- [4] M. Flierl, A. Mavlanckar, and B. Girod, "Motion and disparity compensated coding for multiview video," in *IEEE Transactions on Circuits and Systems for Video Technology*, vol. 17, no.11, November 2007, pp. 1474–1484.
- [5] P. Merkle, A. Smolic, K. Mueller, and T. Wiegand, "Multi-view video plus depth representation and coding," in *IEEE International Conference on Image Processing*, San Antonio, TX, October 2007.
- [6] M. Tanimoto, T. Fujii, K. Suzuki, N. Fukushima, and Y. Mori, "Reference softwares for depth estimation and view synthesis," in *ISO/IEC JTC1/SC29/WG11 MPEG2008/M15377*, Archamps, April 2008.
- [7] D. Tian, P.-L. Lai, P. Lopez, and C. Gomila, "View synthesis techniques for 3D video," in *Applications of Digital Image Processing XXXII, Proceedings of the SPIE*, vol. 7443 (2009), 2009, pp. 74 430T–74 430T–11.
- [8] S. Gokturk, H. Yalcin, and C. Bamji, "A time-of-flight depth sensor—system description, issues and solutions," in *Conference on Computer Vision and Pattern Recognition Workshop (CVPRW)*, Washington, DC, June 2004.
- [9] T. Maugey, P. Frossard, and G. Cheung, "Temporal and view constancy in an interactive multiview streaming system," in *Proc. of the IEEE International Conference on Image Processing*, Orlando, FL, September 2012.
- [10] I. Daribo, G. Cheung, T. Maugey, and P. Frossard, "RD optimized auxiliary information for inpainting-based view synthesis," in *3DTV-Conference 2012*, Zurich, Switzerland, October 2012.
- [11] K.-J. Oh, S. Yea, and Y.-S. Ho, "Hole-filling method using depth based inpainting for view synthesis in free viewpoint television (FTV) and 3D video," in *Picture Coding Symposium*, Chicago, IL, May 2009.
- [12] I. Daribo and B. Pesquet-Popescu, "Depth-aided image inpainting for novel view synthesis," in *IEEE International Workshop on Multimedia and Signal Processing*, Saint-Malo, France, October 2010.
- [13] E. Kurutepe, M. R. Civanlar, and A. M. Tekalp, "Client-driven selective streaming of multiview video for interactive 3DTV," in *IEEE Transactions on Circuits and Systems for Video Technology*, vol. 17, no.11, November 2007, pp. 1558–1565.
- [14] "Voxel," <http://www.wikipedia.org/wiki/Voxel>.
- [15] Y. Chen, Y. Hu, O. Au, H. Li, and C. W. Chen, "Video error concealment using spatio-temporal boundary matching and partial differential equation," in *IEEE Transactions on Multimedia*, vol. 10, no.1, January 2008, pp. 2–15.
- [16] C. Yeo, W. t. Tan, and D. Mukherjee, "Receiver error concealment using acknowledge preview (RECAP)—an approach to resilient video streaming," in *IEEE International Conference on Acoustics, Speech and Signal Processing*, Taipei, Taiwan, April 2009.
- [17] P. Merkle, A. Smolic, K. Muller, and T. Wiegand, "Efficient prediction structures for multiview video coding," in *IEEE Transactions on Circuits and Systems for Video Technology*, vol. 17, no.11, November 2007, pp. 1461–1473.
- [18] *Video Coding for Low Bitrate Communication*, ITU-T Recommendation H.263, February 1998.
- [19] T. Wiegand, G. Sullivan, G. Bjontegaard, and A. Luthra, "Overview of the H.264/AVC video coding standard," in *IEEE Transactions on Circuits and Systems for Video Technology*, vol. 13, no.7, July 2003, pp. 560–576.
- [20] Y. Zhang and Z. Xiong, "On the sum-rate loss of quadratic gaussian multiterminal source coding," in *IEEE Transactions on Information Theory*, vol. 57, no.9, September 2011, pp. 5588–5614.
- [21] G. Shen, W.-S. Kim, S. Narang, A. Ortega, J. Lee, and H. Wey, "Edge-adaptive transforms for efficient depth map coding," in *IEEE Picture Coding Symposium*, Nagoya, Japan, December 2010.
- [22] J. Gautier, O. L. Meur, and C. Guillemot, "Depth map coding: exploiting the intrinsic properties of scenes and surface layout," in *Picture Coding Symposium 2012*, Krakow, Poland, May 2012.
- [23] W. Hu, G. Cheung, X. Li, and O. Au, "Depth map compression using multi-resolution graph-based transform for depth-image-based rendering," in *Proc. of the IEEE International Conference on Image Processing*, Orlando, FL, September 2012.
- [24] W.-S. Kim, A. Ortega, P. Lai, D. Tian, and C. Gomila, "Depth map distortion analysis for view rendering and depth coding," in *IEEE International Conference on Image Processing*, Cairo, Egypt, November 2009.
- [25] —, "Depth map coding with distortion estimation of rendered view," in *SPIE Visual Information Processing and Communication*, San Jose, CA, January 2010.
- [26] G. Cheung, A. Kubota, and A. Ortega, "Sparse representation of depth maps for efficient transform coding," in *IEEE Picture Coding Symposium*, Nagoya, Japan, December 2010.
- [27] G. Cheung, J. Ishida, A. Kubota, and A. Ortega, "Transform domain sparsification of depth maps using iterative quadratic programming," in *IEEE International Conference on Image Processing*, Brussels, Belgium, September 2011.
- [28] G. Valenzise, G. Cheung, R. Galvao, M. Cagnazzo, B. Pesquet-Popescu, and A. Ortega, "Motion prediction of depth video for depth-image-based rendering using don't care regions," in *Picture Coding Symposium 2012*, Krakow, Poland, May 2012.
- [29] P. Merkle, C. Bartnik, K. Muller, D. Marpe, and T. Wiegand, "3D video: Depth coding based on inter-component prediction of block partitions," in *2010 Picture Coding Symposium*, Krakow, Poland, May 2012.
- [30] I. Daribo, D. Florencio, and G. Cheung, "Arbitrarily shaped sub-block motion prediction in texture map compression using depth information," in *2010 Picture Coding Symposium*, Krakow, Poland, May 2012.
- [31] B. Macchiavello, C. Dorea, M. Hung, G. Cheung, and W. t. Tan, "Reference frame selection for loss-resilient texture and depth map coding in multiview video conferencing," in *Proc. of the IEEE International Conference on Image Processing*, Orlando, FL, September 2012.
- [32] R. Li, D. Rusanovskyy, M. Hannuksela, and H. Li, "Joint view filtering for multiview depth map sequences," in *IEEE International Conference on Image Processing*, Orlando, FL, October 2012.
- [33] H. Furihata, T. Yendo, M. Tehrani, T. Fujii, and M. Tanimoto, "Novel view synthesis with residual error feedback for ftv," in *IS&T/SPIE Stereoscopic Displays and Applications XXI*, vol. 7524, 2010, pp. 75 240K–75 240K.
- [34] H. Helgason, H. Li, and M. Flierl, "Multiscale framework for adaptive and robust enhancement of depth in multi-view imagery," in *IEEE International Conference on Image Processing*, Orlando, FL, October 2012.
- [35] Y. Wang and Q.-F. Zhu, "Error control and concealment for video communication: A review," *IEEE Proceedings*, vol. 86, pp. 974–997, 1998.
- [36] Y. Wang, M. Claypool, and R. Kinicki, "modeling RPS and evaluating video repair with VQM," *IEEE Trans. Multimedia*, vol. 11, no. 1, pp. 128–37, 2009.
- [37] G. Cheung, W.-T. Tan, and C. Chan, "Reference frame optimization for multiple-path video streaming with complexity scaling," in *IEEE Transactions on Circuits and Systems for Video Technology*, vol. 17, no.6, June 2007, pp. 649–662.
- [38] E. Martinian and M. Trott, "Delay-optimal burst erasure code construction," in *IEEE Int. Symp. on Info. Theory*, Nice, France, June 2007.
- [39] P. Lambert, W. Neve, Y. Dhondt, and R. Walle, "Flexible macroblock ordering in h.264/avc," in *J. of Visual Comm. & Image Representation*, vol. 17, 2006.
- [40] T. Stockhammer and M. Bystrom, "H.264/AVC data partitioning for mobile video communication," in *IEEE International Conference on Image Processing*, October 2004.
- [41] T. Troger, "Inter-sequence error concealment techniques for multi-broadcast tv reception," *IEEE Trans. Broadcasting*, vol. 57, no. 4, pp. 777–793, 2011.
- [42] Y. Eisenberg, F. Zhai, C. Luna, R. Berry, and A. Katsaggelos, "Variance-aware distortion estimation for wireless video communications," in *ICIP*, September 2003.

- [43] A. Tan, A. Aksay, G. Akar, and E. Arikan, "Rate-distortion optimization for stereoscopic video streaming with unequal error protection," in *EURASIP Journal on Advances in Signal Processing*, 2009.
- [44] C. Hou, R. Pan, Z. Yuan, and L. Yang, "Distortion analysis and error concealment for multiview video transmission," in *IEEE International Symposium on Broadband Multimedia Systems and Broadcasting*, Tianjin, China, March 2010.
- [45] X. Xiu, G. Cheung, and J. Liang, "Delay-cognizant interactive streaming of multiview video with free viewpoint synthesis," in *IEEE Transactions on Multimedia*, vol. 14, no.4, August 2012, pp. 1109–1126.
- [46] B. Macchiavello, C. Dorea, M. Hung, G. Cheung, and W. t. Tan, "Reference frame selection for loss-resilient depth map coding in multiview video conferencing," in *IS&T/SPIE Visual Information Processing and Communication Conference*, Burlingame, CA, January 2012.
- [47] Y. Zhou, C. Hou, W. Xiang, and F. Wu, "Channel distortion modeling for multi-view video transmission over packet-switched networks," in *IEEE Transactions on Circuits and Systems for Video Technology*, vol. 21, no.11, November 2011, pp. 1679–1692.
- [48] MPEG Video Group, "Call for contributions on 3D video test material," in *ISO/IEC JTC1/SC29/WG11 N9595*, Antalya, Turkey, January 2008.
- [49] M. Tanimoto, M. P. Tehrani, T. Fujii, and T. Yendo, "Free-viewpoint TV," in *IEEE Signal Processing Magazine*, vol. 28, no.1, January 2011.
- [50] W. Mark, L. McMillan, and G. Bishop, "Post-rendering 3D warping," in *Symposium on Interactive 3D Graphics*, New York, NY, April 1997.
- [51] H.-Y. Shum, S.-C. Chan, and S. B. Kang, *Image-Based Rendering*. Springer, 2007.
- [52] "Nagoya university ftv test sequences," in <http://www.tanimoto.nuee.nagoya-u.ac.jp/>.
- [53] "JM H.264 reference software v18.0," in <http://iphome.hhi.de/suehring/tml/>.